Electronic Supplementary Information

Adaptively Reconstructing Network of Soft Elastomers to Increase Strand Rigidity: towards Free-Standing Electro-Actuation Strain over 100%

*Zheqi Chen, Zipeng Ma, Jiali Tang, Youhua Xiao, Jie Mao, Yiting Cai, Junjie Zhao, Xiang Gao, Tiefeng Li, and Yingwu Luo**

Email: yingwu.luo@zju.edu.cn

This material includes

Experimental

Table S2 Fitting parameters summary for tensile behaviors of pristine and trained SEHAS.

Table S3 Relative dielectric constant at 0.1 Hz and 1 kHz for pristine and trained SEHAS.

Table S4 Mechanical properties and electro-actuation performance of previously reported DEs.

Table S5 Fitting parameters summary for tensile behaviors of pristine and trained SBAS.

Experimental

Materials: Acrylic acid, styrene and 2-ethylhexyl acrylate were purified by vaccum distillation to remove the inhibitor. Potassium persulfate (KPS, >99%), 4,4'-azobis (4-cyano-pentanoic acid) (V501, >99%), 2,2'-azobis[2-(2-imidazolin-2-yl) propane] dihydrochloride (VA044, >99%), cyclohexane (AR), 1,4-dioxane (AR), tetrahydrofuran (THF, AR), sodium hydroxide (NaOH, AR), sodium dodecyl sulfate (SDS, AR) were used without further purification. All the chemicals above were purchased from Macklin Ltd. 2-(([dodecylsulfanyl]carbonothioyl) sulfanyl) propanoic acid (the small RAFT agent) was synthesized according to the literature.[1] And the macro-RAFT agent (PAA_{20}-PSt_5-RAFT), used as both the RAFT agent and the emulsifier in the RAFT emulsion polymerization,[2] was synthesized according to our previous work.[2] Single wall carbon nanotube (SWCNT) for the fabrication of electrodes was purchased from Aladdin Ltd.

Synthesis of SEHAS triblock copolymer latex: The SEHAS triblock copolymer was synthesized *via* RAFT emulsion polymerization through sequential feeding of monomer styrene and 2-ethylhexyl acrylate accordioning to our previous work.[3] Firstly, 3.22 g macro-RAFT, 21 g styrene, and 94.98 g deionized water were mixed in a 1000 ml flask. Nitrogen purge for 90 minutes at room temperature was used to remove the oxygen in the reaction system, and the flask reactor was placed in a water bath at 80 ^{o}C. The stirring rate was set at 190 rpm. A KPS aqueous solution (0.025 g KPS in 2.0g deionized water) used as initiator was injected in to the flask to start the reation. The reaction of the first block of polystyrene lasted for 60 min, then a NaOH aqueous solution (0.41 g NaOH in 20.0 g deionized water) was injected slowly (1 g min^{-1}) to maintain the stability of the latex. After cooling down to 45 ^{o}C, 379.63 g deionized water, 168 g 2-ethylhexyl acrylate, and a VA044 aqueous solution (initiator, 0.091 g VA044 in 2.0 g deionized water) were then injected into the flask. The reaction time for the second block was 300 min. Then 21 g styrene was injected to the flask and the reaction for the third block lasted for 300 min.

Preparation of elastomer films: Dilute HCl aqueous solution was used for demulsification. The elastomers were washed by deionized water until neutral and dried in vacuum at 120 ^{o}C for 12 hours. An elastomer film was obtained by casting a around 40 ml of 0.1 g mL^{-1} copolymer solution in a PTFE container with a diameter of 100 mm. After slowly evaporating almost all

the solvent, the elastomer film was annealing in at 120 ^{o}C for 24 hours. The thickness of obtained film is around 0.5 mm.

Preparation of SWCNT electrodes: 10 mg SWCNT and 1.8 g SDS were mixed in 180 g deionized water and then ultrasonicated (300 W of power) for 10 min. SWCNT dispersions were obtained from the supernatant after centrifugation and decantation. The dispersion solution was then suction filtered through PVDF microporous membrane with 0.45 μm pore diameter to form a SWCNT layer on the membrane ready for the transfer printing later. The sheet resistance of the electrodes was around 1 kΩ cm^{-2} measured by a four-probe setup.

Characterization: The number-average molecular weight (M_n) and polydispersion index (PDI) were measured by a gel permeation chromatography (GPC, Waters 1525/2414). 3 g L^{-1} copolymer solutions (THF as solvent) were filtered with a 450 nm syringe filter. M_n and PDI are calculated based on the calibration of a narrow polystyrene standard. The composition of the copolymers was determined by ^{1}H NMR (Bruker AVANCE III 500) with THF-d$_8$ as a solvent. The nanomorphology of SEHAS was observed by an atomic force microcopy (AFM, Veeco MultiMode) in a tapping mode. Specimens for AFM were produced by spin-casting a 0.1 g L^{-1} copolymer solution onto a silicon chip at 2000 rpm for 1min and then annealing at 120 ^{o}C for 24 hours. Polarized optical images were taken by a camera (Canon 70D, 100 mm lens) equipped with a polarizer. A white light-emitting diode (LED) screen was used as the polarized background light. Specimens were placed between the LED screen and polarizer in a direction that inclined to the polarization direction for the background light at an angle of 45 degree. SAXS was measured on Xenocs Nano-inXider with an X-ray wavelength of 1.54 nm. The sample-to-detector distance was 936 nm and the exposure time of X-ray was 300 s in SAXS measurement. The elastomer films were cut into dumbbell-shaped specimens for tensile test with a neck length of 20 mm and a neck width of 2 mm. The uniaxial tensile behaviors were measured by a universal testing machine (Zwick/Roell Z020) with a constant rate of 100 % min^{-1} at room temperature. The dielectric constant in the frequency range from 10^{-1} Hz to 10^{7} Hz at 25 ^{o}C was measured by a broadband dielectric spectrometer (Novocontrol Concept40). The specimen cut by laser with a diameter of 10 mm was sandwiched with two stainless steel electrodes with 10 mm diameter. The film was slightly compressed during the measurement to ensure good contract between electrodes and the film. The distance between the two electrodes

measured by a micrometer gauge was taken as film thickness. The experimental errors (~10%) in dielectric measurements came from the errors of film thickness due to the softness of elastomers. The dynamic mechanical properties were measured by Dynamic Mechanical Analyzer (DMA, TA Q800) in the tensile mode with 1 Hz operating frequency and 15 μm operating amplitude. The testing temperature range was from -70 ^{o}C to 100 ^{o}C with a constant heating rate of 3 ^{o}C min^{-1}.

Free-standing electro-actuation test: Electro-actuation performance was conducted using a diaphragm actuator at a prestrain-free condition according to an accepted standard. The elastomer films were placed into two rigid acrylic rings with 10 mm inner diameter, and the bottom ring stuck tightly onto the top of a diaphragm chamber. A controlled bias air pressure of 1.0-1.5 kPa was used to guide the direction of actuation strain (out of plane). The diameter of active area was 10 mm (before the actuation and the set of bias air pressure) with two SWCNT electrodes on the both side of an elastomer film. A high-voltage power supply (Trek 610E) was used to drive the actuators. Images and video of actuation were obtained by a camera (Canon 70D, 100 mm lens). The actuation strain was calculated by analyzing the images by Adobe Photoshop.

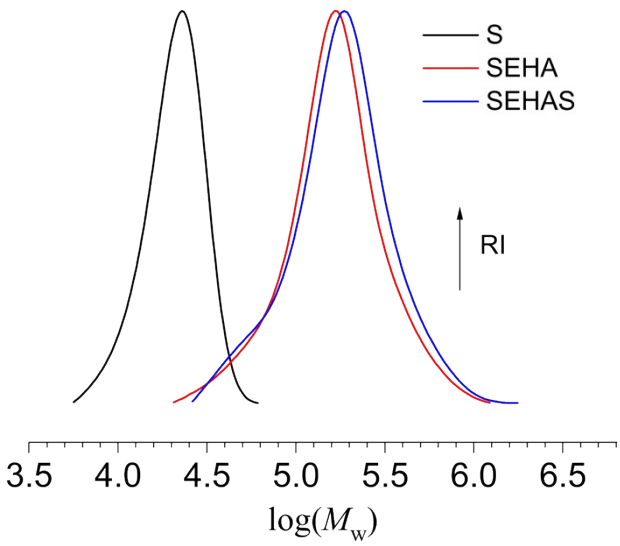

Fig. S1 Evolution of GPC curves in the end of each block formation during the synthesis of the triblock copolymer SEHAS. The formation of the triblock structure is confirmed by GPC curve movement as a whole to higher molecular weight after chain extension.

Table S1 Polymerization results for each block of the designed triblock copolymer SEHAS.

Sample	Conv[a](%)	$M_{n,design}$(kg/mol)	$M_{n,exp}$[b](kg/mol)	PDI[c]
S	96	15	19.3	1.15
SEHA	95	135	136.6	1.48
SEHAS	95	150	146.2	1.52

[a]Monomer conversion of each block synthesis estimated by gravimetric analysis. [b]Number-average molecular weight $M_{n,exp}$ and [c]polydispersity index values were determined by Gel Permeation Chromatography.

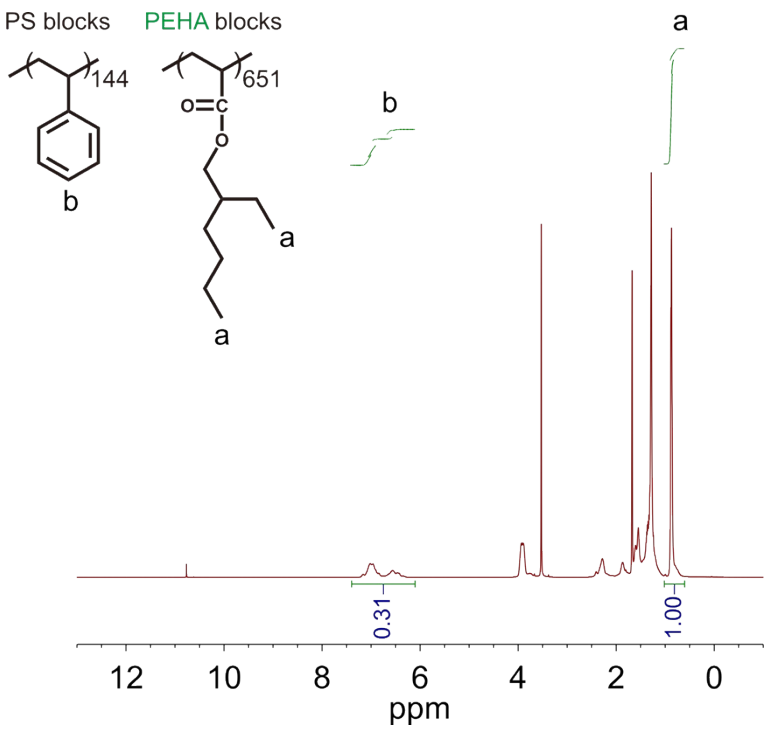

Fig. S2 ^{1}H NMR spectra (The signals from hydrogen of phenyl groups and the signals from hydrogen of methyl groups were used to calculate the composition of the copolymers). The calculated polystyrene composition from ^{1}H NMR spectra is 17.4 *wt.*%. The presence of carboxylic acid groups is due to the use of macro-RAFT agent (PAA_{20}-PSt_5-RAFT).

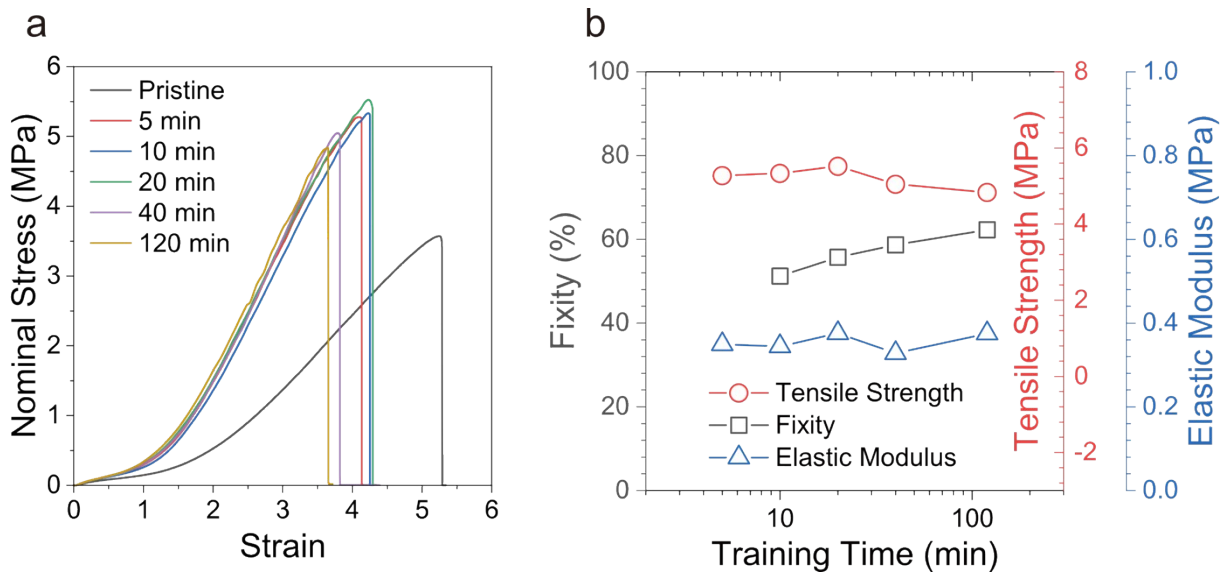

Fig. S3 Effect of different training time on mechanical performance and fixity of SEHAS. The equal-biaxial stretch ratio D/D_0 is chosen as 2.0. a) Uniaxial nominal stress curves for specimens with different training time. All the trained specimens show more intense strain-hardening behaviors than the pristine specimen. The tensile behaviors of specimens with different training time are almost the same. b) As the increase of training time, the fixity (defined as the thickness change ratio, $\text{Fixity} = \frac{H_{\text{trained}}}{4H_0} \times 100\%$ where H_{trained} is the film thickness after training and H_0 is the pristine film thickness) gradually increases, but the tensile strength and elastic modulus remain almost unchanged. The fixity for specimens with 5 minutes of training time cannot be calculated due to the thickness uniformity caused by uneven heating in the elastomer film. To eliminate the influence of uneven heating, 20 minutes for training time is used in this work.

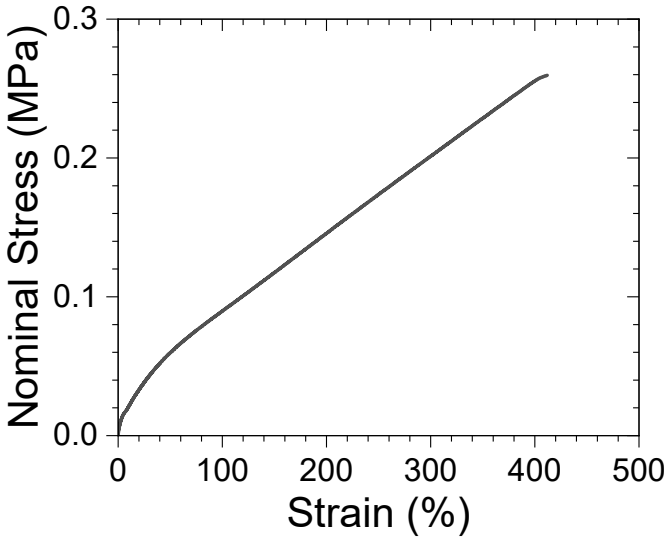

Fig. S4 Uniaxial tensile curve for pristine SEHAS at 90 ^{o}C measured by DMA.

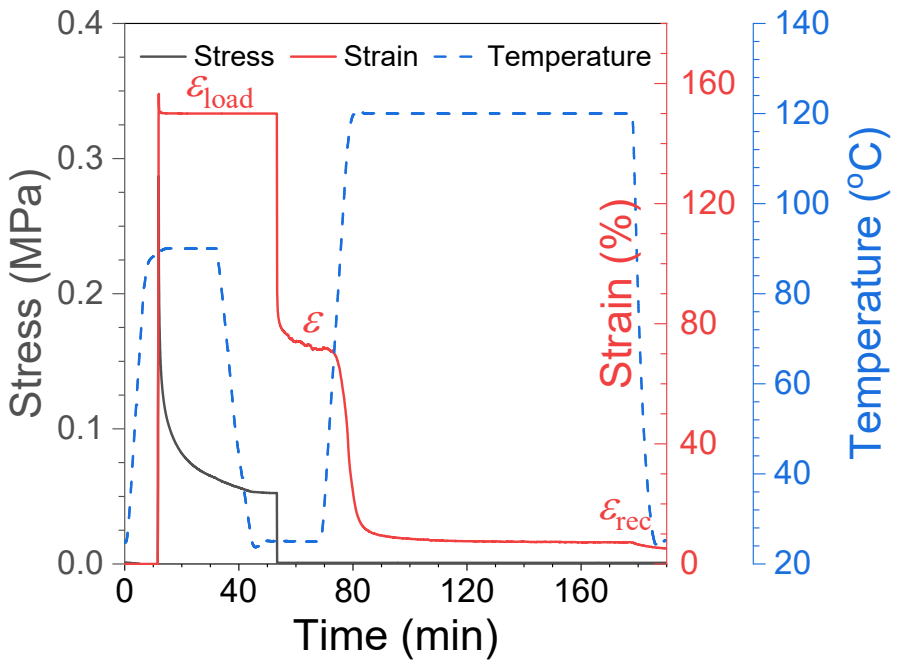

Fig. S5 A model experiment to evaluate the shape memory behavior measured by a dynamic mechanical analyzer (DMA, TA Q800). A specimen with a size of 5×20 mm and thickness around 0.5 mm is cut by laser. The programming is conducted at 90 °C for 20 min (the same condition used in the thermomechanical training process) and with a uniaxial strain of 150%. The fixity is defined as $R_f = \frac{\varepsilon}{\varepsilon_{load}} \times 100\% = 48.6\%$ and the recovery ratio is defined as $R_r = \frac{\varepsilon - \varepsilon_{rec}}{\varepsilon} \times 100\% = 93.1\%$.

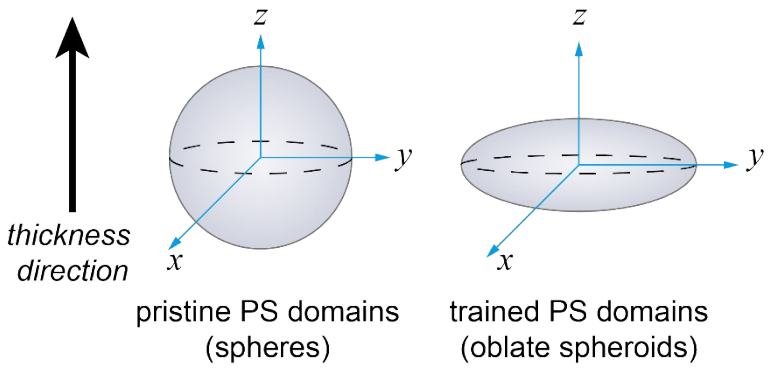

Fig. S6. Schematic illustration of the change of PS domain morphology after training, here *z*-axis is thickness direction. The morphology changes from spheres to oblate spheroids after thermomechanical training due to the force-induced orientation with expansion in the area (*x*-*y* plane) and contraction in thickness. Thermomechanically induced PS domain morphology change was also reported in our previous works.[4, 5]

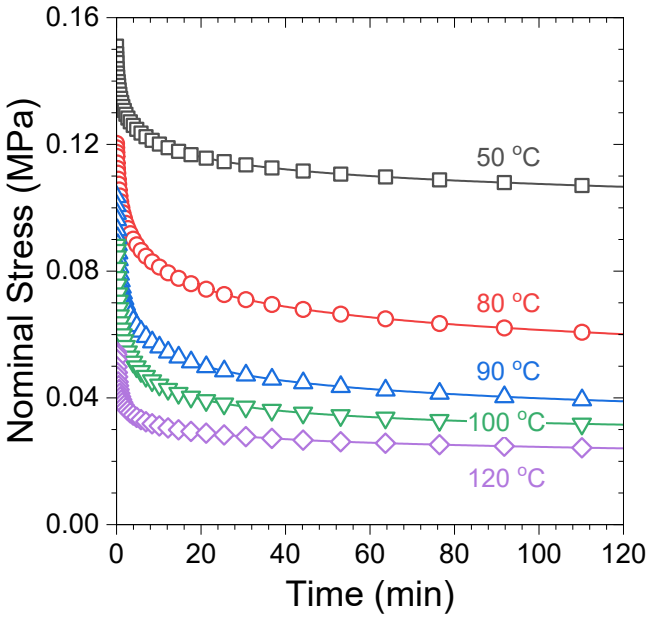

Fig. S7 Stress relaxation curves for SEHAS elastomers at different temperature, measured by a dynamic mechanical analyzer (DMA, TA Q800). Specimens with a size of 5×20 mm and thickness around 0.5 mm is cut by laser. The strain is set at 150 %. Part of stress cannot be relaxed during the testing period of 2 hours even the heating temperature is higher than T_g of polystyrene (~100 °C).

Table S2. Fitting parameters summary for Equation 1 in the main manuscript.

Sample	Pritine	D/D_0 = 1.5	D/D_0 = 2.0	D/D_0 = 2.5
E_s	0.198	0.207	0.229	0.234
β	0.146	0.194	0.256	0.331

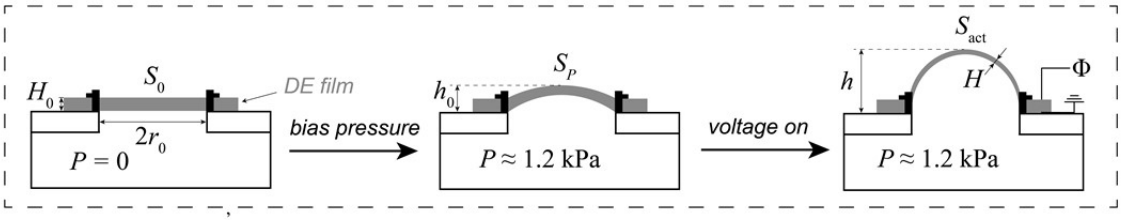

Fig. S8 Strain calculation of free-standing electro-actuation. The testing and calculating method are referred to a well-accepted standard.[6] Area expansion is calculated by $\lambda_a = \frac{S_{act}}{S_0} = \frac{h^2 + r_0^2}{r_0^2}$. The area strain s_{area} used to calculate the energy density (deducting the contribution of air pressure) is defined as $s_{area} = \frac{S_{act}}{S_P} = \left(\frac{r_0^2 + h^2}{r_0^2 + h_0^2} - 1\right) \times 100\%$. The calculated air-pressure-induced strain is around 15% to lead the direction of actuation.

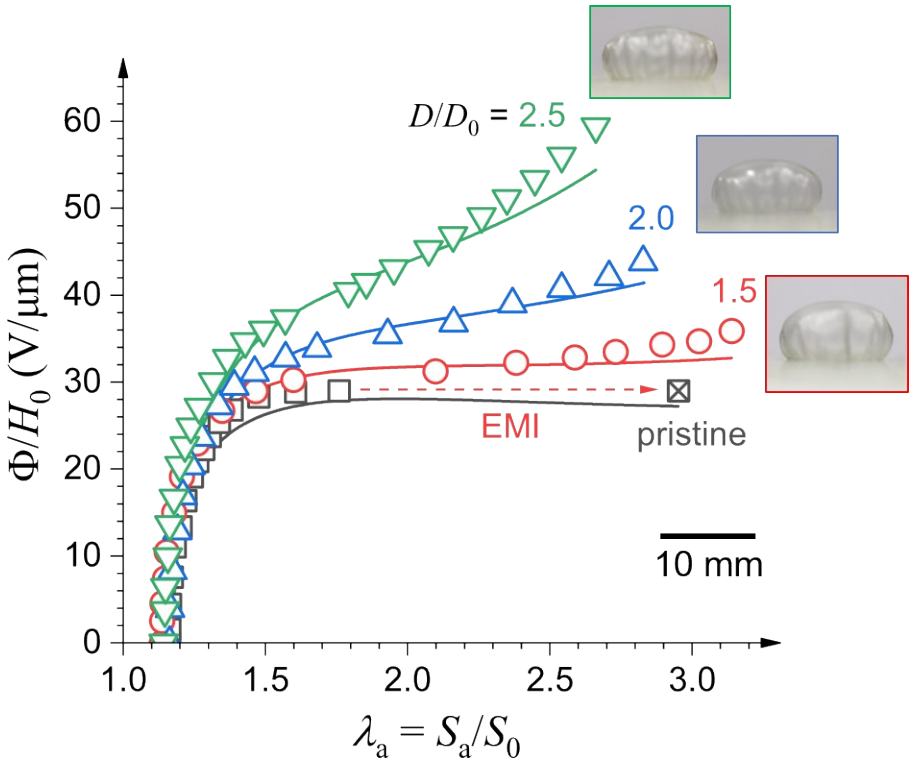

Fig. S9 Electro-actuation for pristine and trained SEHAS. The experimental data is consistent with the theoretical prediction (solid lines) by $\Phi / H_0 = \frac{1}{\sqrt{\varepsilon\varepsilon_0}} \sqrt{-\lambda^2 \sigma_{\text{true}}(\lambda) - \frac{Pr_0}{4H_0\sqrt{\lambda^{-1}-1}}}$ [7] where $\sigma_{\text{true}}(\lambda)$ is referred to $\sigma_{\text{true}} = \frac{E}{9}\left(\lambda^2 - \lambda^{-1}\right)\left[1 + 2\left(1 - \frac{\beta(\lambda^2 + 2/\lambda)}{3}\right)^{-2}\right]$ [7], and $\lambda = H / H_0 = \lambda_a^{-1}$.

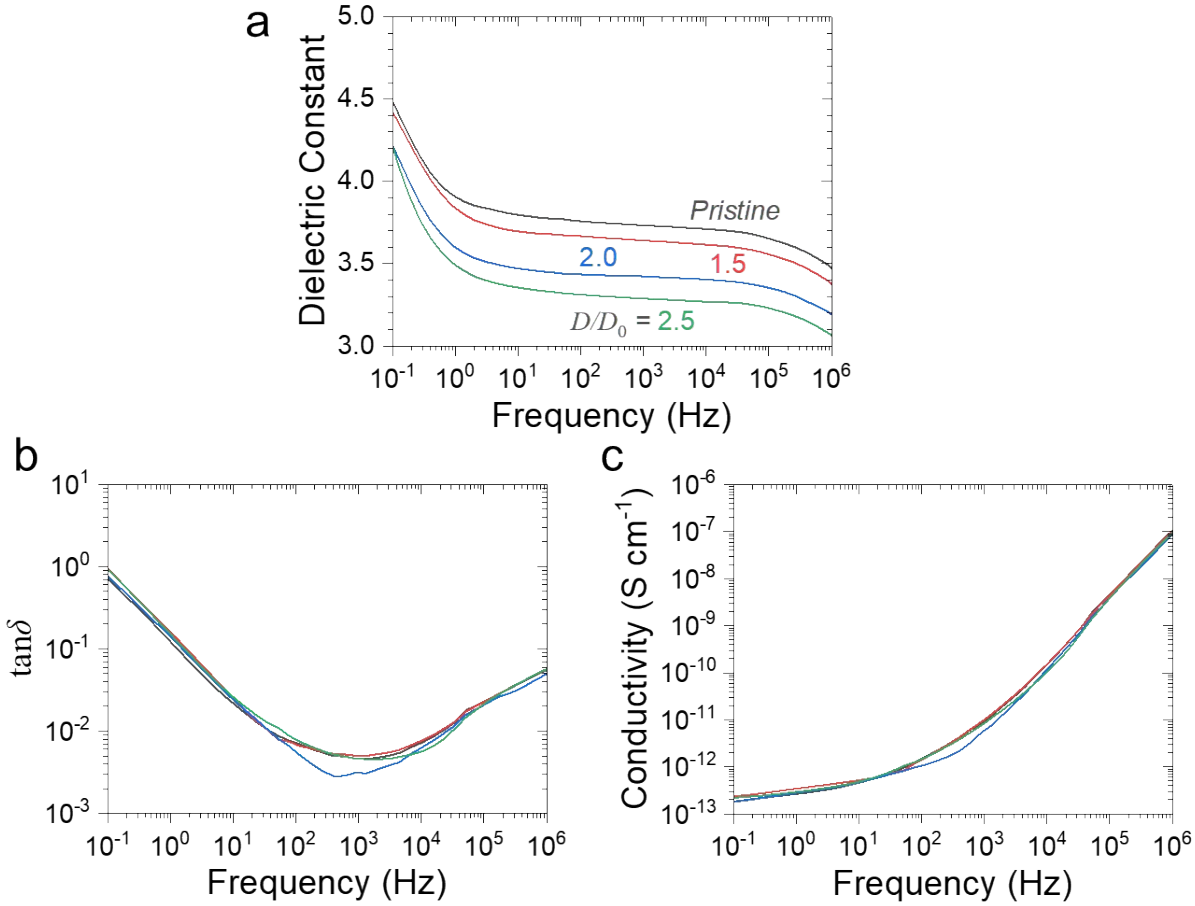

Fig. S10 Dielectric properties: a) relative dielectric constant, b) dielectric loss tangent, and c) conductivity. The relative dielectric constant of the SEHAS film decreases slightly after thermomechanical training. Part of network strands remain inner stretch after training. As a result, part of 2-ethylhexyl acrylate units composing the backbone should be oriented in the direction of stretching thus the dipoles (ester groups) loose part of their freedom in the electro-orientation.[9] In the low frequencies, the relative permittivity quickly increases due to the interfacial polarization effect.

Table S3. Relative dielectric constant at 0.1 Hz and 1 kHz.

Sample	Pritine	D/D_0 = 1.5	D/D_0 = 2.0	D/D_0 = 2.5
ε (at 0.1 Hz) [a)]	4.49	4.43	4.22	4.22
ε (at 1 kHz)	3.73	3.64	3.42	3.28

a) In the theoretical prediction of electro-actuation behaviors (solid curves in Fig. 4b and Fig. S9), the values of relative dielectric constant are obtained at frequency of 0.1 Hz since the voltage rise is very slow. Except that, the values of dielectric constant reported in this manuscript are obtained at frequency of 1 kHz.

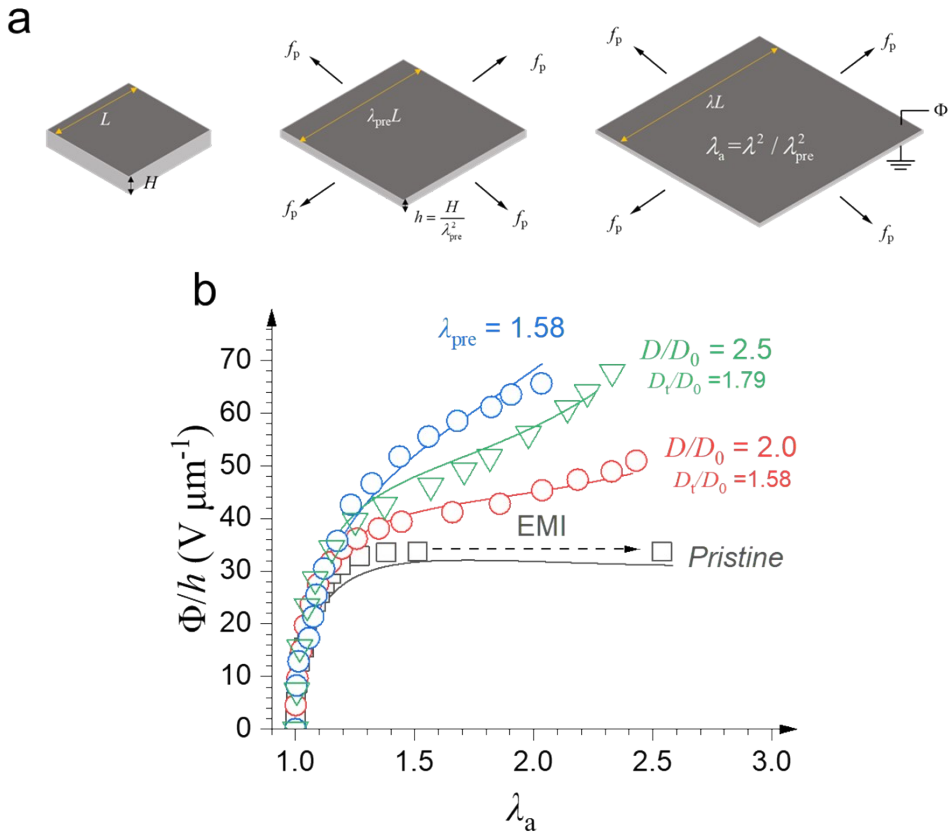

Fig. S11 a) Schematic diagram of a dielectric elastomer actuator by the pre-stretch method. The elastomer film was stretched by an equal biaxial force f_p to the target stretch ratio λ_{pre} then clamped between two rigid rings. The diameter active region (8 mm) is much smaller than that of the inner diameter of the rigid rings (50 mm) to prevent the loss of tension.[10] area expansion $\lambda_a = \lambda^2 / \lambda_{pre}^2$ is the calculated by the area change of the active region. b) Electro-actuation behaviors of the pre-stretched SEHAS (bracing on rigid frames) and trained SEHAS with the same final dimension ($\lambda_{pre} = D_t/D_0$). The solid lines are theoretical predictions.

The pre-stretch method uses the external frame to lock the stretched state of network strands and thus can eliminate EMI. As a comparison, the thermomechanical training method uses the in-situ generated second network to lock the stretched chain, so the rigid frames can be removed. At the same electric field, the trained SEHAS exhibits a larger deformation than that of pre-stretched SEHAS due to its lower modulus. The lower modulus of trained SEHAS is due to that part of network strands are relaxed to form a second network during training while all the network strands in pre-stretched SEHAS are in tension after pre-strain.

Theoretical predictions for the electro-actuation behaviors of the pre-stretched sample

The external equal-biaxial force can be seen as a constant value of f_p since the active region is much smaller than that of the inner diameter of the rigid rings. So, at each force equilibrium state[11]:

$$\lambda \frac{f_p}{LH} + \varepsilon \left(\lambda^2 \frac{\Phi}{H} \right)^2 = \sigma_{true}(\lambda)$$

where $\sigma_{pre} = \frac{f_p \lambda_{pre}}{LH}$, $H = h\lambda_{pre}^2$. One can derive the relation between $\frac{\Phi}{h}$ and λ as:

$$\frac{\Phi}{h} = \lambda_{pre}^2 \lambda^{-2} \sqrt{\frac{\sigma_{true}(\lambda) - \lambda \left(\frac{\sigma_{pre}}{\lambda_{pre}} \right)}{\varepsilon}}$$

where $\lambda = \lambda_{pre}\sqrt{\lambda_a}$. It should be noted that dielectric constant will decrease after pre-stretch, here we estimate the dielectric constant is 0.82 times that of pristine SEHAS according to the literature.[12]

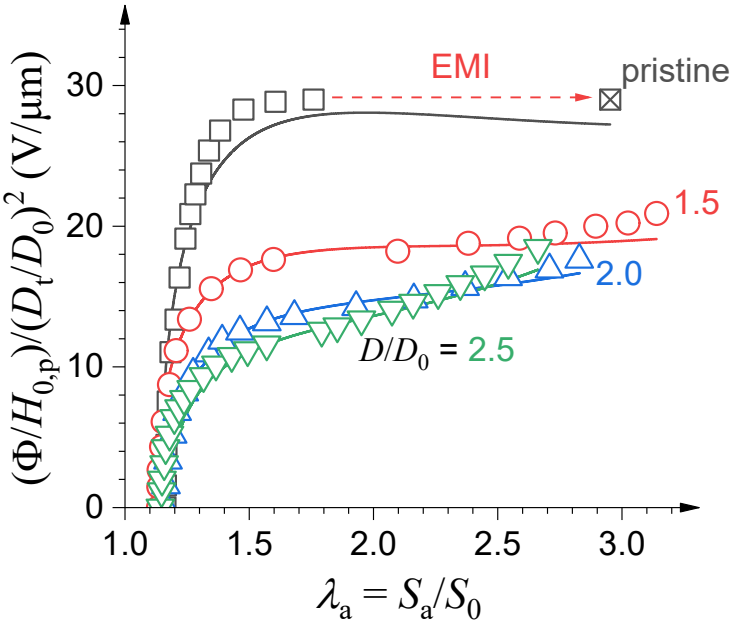

Fig. S12 Electro-actuation relation for pristine and trained SEHAS when considering film thickness reduction. $H_{0,p}$ is the thickness of the pristine SEHAS film. After thermomechanical training, the film thickness is reduced by a factor of $(D_t/D_0)^2$, the square of the "plastic deformation". The results illustrate that the current training method can decrease the actuating voltage by accompanied film thickness reduction.

Table S4. Mechanical properties and electro-actuation performance of previously reported materials with over 100% actuation area strain at prestrain-free conditions and those of this work.

Material	Trained SEHAS [a)]	Bottlebrush elastomers [b)]	Plastomers [c)]	IPN(VHB) [d)]	UV-DE [e)]
T_g [f)]/°C	-39	-	-	1	-3
tanδ [g)](@ 25 °C)	0.19	-	-	0.64	0.17
E_0 (MPa)	0.53	0.0045	0.0039	2.4	0.84
σ_{true} (MPa)	25.0	0.027	0.017	-	17.5
ε_b [h)](%)	320	190	120	-	170
ε_r @ 1kHz	3.28	2.94	2.94	4.8	5
$s_{area,max}$ (%)	133	300	224	135	123
E_b (V/μm)	158.1	31.8	31.7	224.0	157.3
e_{max} (kJ/m^3)	307	18	15	911	439

The representative data from this work and that from the literature (completely eliminating EMI): a) Trained SEHAS with D/D_0 = 2.5. b) Bottlebrush elastomer with n_x = 200 (DP of the backbone) and n_{sc} = 28 (DP of the side chains).[7] c) LBL plastomer (sample name: 900-2).[13] d) IPN(VHB) (sample name: w/ 20.16 %).[14] e) UV-DE (sample name: C2-P0).[15] f) T_g is defined by the corresponding temperature of tanδ peak in DMA curves. g) Mechanical loss tangent measured by DMA at 25 °C, 1 Hz. h) Elongation at break.

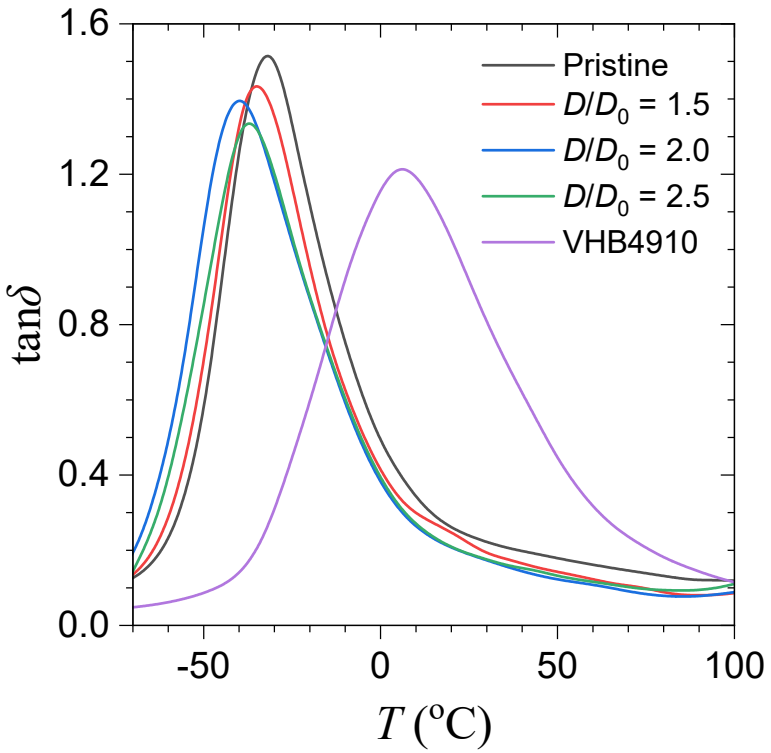

Fig. S13. Mechanical loss tangent tanδ of trained SEHAS with different training stretch ratio and VHB 4910 as a function of temperature (at 1 Hz).

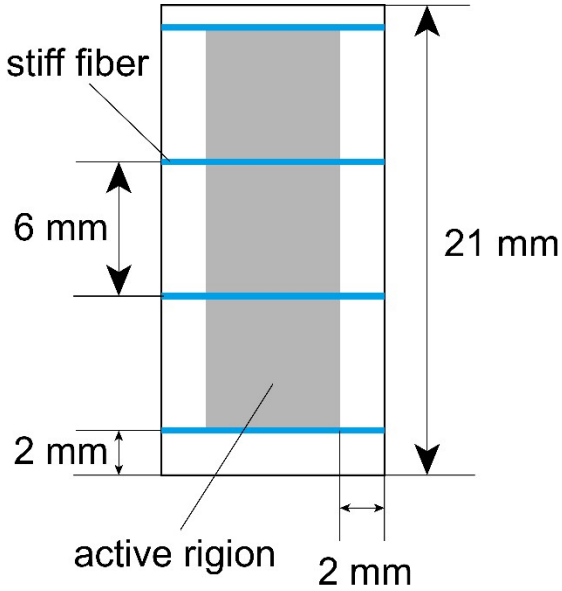

Fig. S14. The structure of the bending actuator. The stiff fibers are placed between the DE layer and the passive layer (PET) to achieve a anistropic actuation strain.[16] The low-temperature environment was created by a jacketed cooler with low-temperature alcohol as the cooling medium.

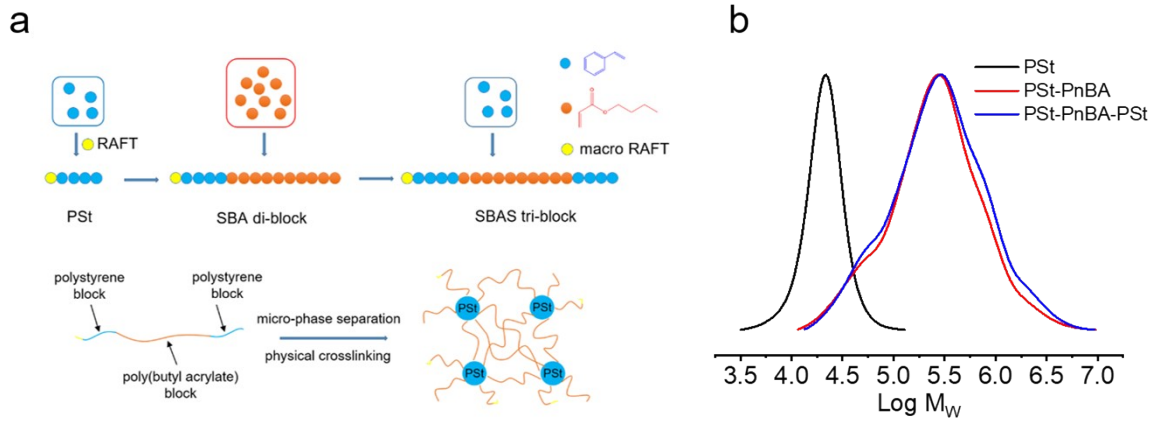

Fig. S15. Schematic illustration for the chain block architecture of SBAS. a) The synthesis of triblock copolymer elastomer SBAS, which is referred to our previous work.[17] b) Evolution of GPC curves in the end of each block formation during the synthesis of SBAS. The PBA chains have smaller alkyl side groups than that of PEHA and thus SBAS own a more flexible network.[18]

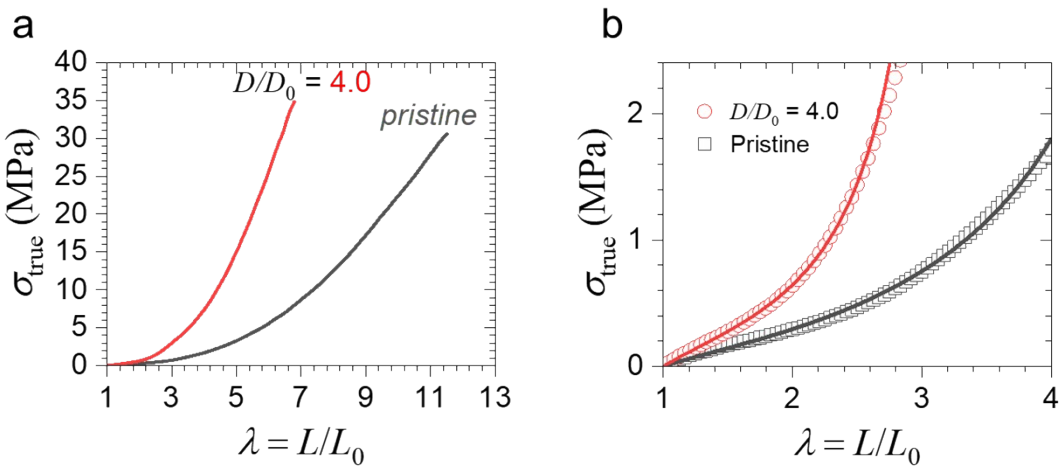

Fig. S16 Tensile behavior for pristine and trained SBAS (D/D_0 = 4.0). a) The uniaxial tensile curves b) The experimental dots of uniaxial tensile curves fitted by $\sigma_{true} = \frac{G}{3}\left(\lambda^2 - \lambda^{-1}\right)\left[1 + \frac{3G_e}{G\lambda} + 2\left(1 - \frac{\beta(\lambda^2 + 2/\lambda)}{3}\right)^{-2}\right]$,[8] where G is the structural shear modulus, G_e is entanglement-contributed shear modulus, and $\beta = \left\langle R_{in}^2 \right\rangle / R_{max}^2$ is the strand extension ratio. Fitting results are the solid curves in the Fig. S16b.

Table S5. Fitting parameters summary for Fig. S16b.

Sample	Pritine SBAS	Trained SBAS with D/D_0 = 4.0
G	0.0460	0.0667
G_e	0.0585	0.1080
β	0.0721	0.2152

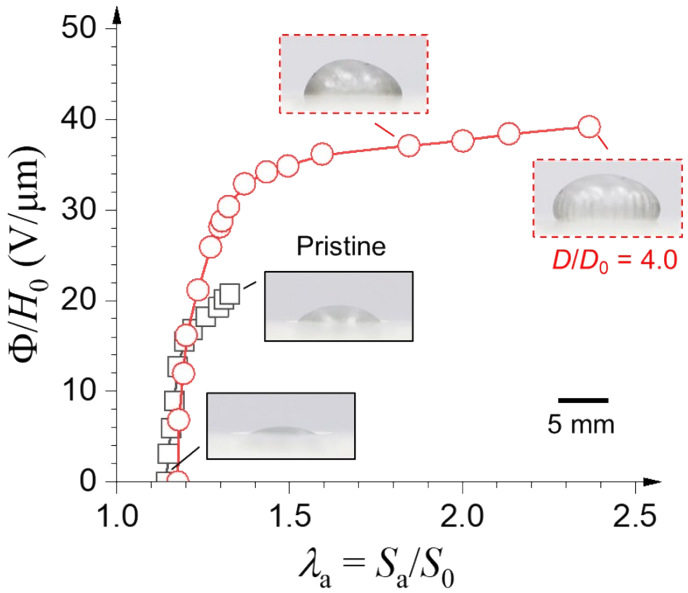

Fig. S17 Electro-actuation for pristine and trained SBAS (D/D_0 = 4.0). The trained SBAS can eliminate EMI to achieve a large electro-actuation area strain of 101%.

References

1. M. J. Monteiro and J. de Barbeyrac, *Macromolecules*, 2001, **34**, 4416.
2. X. Wang, Y. Luo, B. Li and S. Zhu, *Macromolecules*, 2009, **42**, 6414.
3. Z. Chen, Y. Xiao, J. Fang, J. He, Y. Gao, J. Zhao, X. Gao and Y. Luo, *Chem. Eng. J.*, 2021, **405**, 126634.
4. Y. Xiao, Z. Chen, J. Mao, X. Cao, J. He, T. Yang, L. Chen, X. Yang, J. Zhao, T. Li and Y. Luo, *Macromol. Mater. Eng.*, 2021, **306**, 2000732.
5. Y. Xiao, J. Mao, Y. Shan, T. Yang, Z. Chen, F. Zhou, J. He, Y. Shen, J. Zhao, T. Li and Y. Luo, *Nanoscale*, 2020, **12**, 7514.
6. F. Carpi, I. Anderson, S. Bauer, G. Frediani, G. Gallone, M. Gei, C. Graaf, C. Jean-Mistral, W. Kaal, G. Kofod, K. Matthias, K. Roy, L. Benny, M. Marc, M. Silvain, N. Stephan, O. Benjamin, Q. Pei, P. Ron, R. Björn, R. Samuel and S. Herbert, *Smart Mater. Struct.*, 2015, **24**, 105025.
7. M. Vatankhah Varnoosfaderani, W. F. Daniel, A. P. Zhushma, Q. Li, B. J. Morgan, K. Matyjaszewski, D. P. Armstrong, R. J. Spontak, A. V. Dobrynin and S. S. Sheiko, *Adv. Mater.*, 2017, **29**, 1604209.
8. A. V. Dobrynin and J. Y. Carrillo, *Macromolecules*, 2011, **44**, 140.
9. J. Qiang, H. Chen and B. Li, *Smart Mater. Struct.*, 2012, **21**, 25006.
10. S. J. A. Koh, T. Li, J. Zhou, X. Zhao, W. Hong, J. Zhu and Z. Suo, *J. Polym. Sci. B. Poly. Phys.*, 2011, **49**, 504.
11. T. Lu, J. Huang, C. Jordi, G. Kovacs, R. Huang, D. R. Clarke and Z. Suo, *Soft Matter*, 2012, **8**, 6167.
12. J. Qiang, H. Chen and B. Li, *Smart Mater. Struct.*, 2012, **21**, 25006.
13. V. Karimkhani, M. Vatankhah-Varnosfaderani, A. N. Keith, E. Dashtimoghadam, B. J. Morgan, M. Jacobs, A. V. Dobrynin and S. S. Sheiko, *ACS Appl. Polym. Mater.*, 2020, **2**, 1741.
14. S. M. Ha, W. Yuan, Q. Pei, R. Pelrine and S. Stanford, *Adv. Mater.*, 2006, **18**, 887.
15. X. Niu, H. Stoyanov, W. Hu, R. Leo, P. Brochu and Q. Pei, *J. Polym. Sci. B. Poly. Phys.*, 2013, **51**, 197.

16. S. Shian, K. Bertoldi and D. R. Clarke, *Adv. Mater.*, 2015, **27**, 6814.

17. Z. Ma, Y. Xie, J. Mao, X. Yang, T. Li and Y. Luo, *Macromol. Rapid Comm.*, 2017, **38**, 1700268.

18. T. Li, H. Li, H. Wang, W. Lu, M. Osa, Y. Wang, J. Mays and K. Hong, *Polymer*, 2021, **213**, 123207.